

# Even-odd parity transition in strongly correlated locally noncentrosymmetric superconductors : An application to CeRh<sub>2</sub>As<sub>2</sub>

Kosuke Nogaki<sup>1,\*</sup> and Youichi Yanase<sup>1</sup>

<sup>1</sup>*Department of Physics, Kyoto University, Kyoto 606-8502, Japan*

(Dated: June 10, 2022)

The discovery of the multiple  $H$ - $T$  phase diagram of CeRh<sub>2</sub>As<sub>2</sub> offers a new route to designing topological superconductors. Although weak-coupling theories explain the experimental phase diagram qualitatively, a quantitative discrepancy between them has discouraged conclusive interpretation. In this Letter, we thoroughly study the effect of Coulomb interaction and the phase diagrams of locally noncentrosymmetric superconductors. We reveal even-odd parity transition and the enhancement of the parity transition field in strongly correlated superconductors, and an issue of CeRh<sub>2</sub>As<sub>2</sub> is resolved.

*Introduction.* — Searching for odd-parity superconductors has been a central issue in designing topological materials [1–4]. Due to Fermi statistics, odd-parity superconductors are classified into spin-triplet superconductors within the theory by Bardeen, Cooper, and Schrieffer (BCS) [5], which brilliantly explains various phenomena of superconductivity. In the topological science, this constraint on Cooper pairs has led to the renewed interest in uncommon spin-triplet superconductors such as UPt<sub>3</sub> [6–9], UCoGe [10–12], and UTe<sub>2</sub> [13–16]. However, some internal degrees of freedom of Cooper pairs are overlooked in the canonical BCS theory.

Recently, the local noncentrosymmetry in superconductors has attracted much attention and shed light on the sublattice degree of freedom in Cooper pairs [17–31]. Interestingly, the sublattice antisymmetric Cooper pair is allowed, leading to an odd-parity superconducting state without spin-triplet pairs. Therefore, the sublattice degree of freedom paves a new way to design topological odd-parity superconductors based on pairing in the ordinary spin-singlet channel [22, 32]. In the high-magnetic field phase of locally noncentrosymmetric superconductors, the sublattice antisymmetric superconducting state is theoretically predicted to be thermodynamically stable and named the pair-density-wave (PDW) state [19].

The discovery of the two superconducting phases in the  $H$ - $T$  phase diagram of CeRh<sub>2</sub>As<sub>2</sub> [33] has led attention to the sublattice degree of freedom in superconductors [32–46]. In fact, due to the fascinating crystalline structure of CeRh<sub>2</sub>As<sub>2</sub>, the inversion symmetry is locally broken at the Ce site but globally preserved [33]. The qualitative similarity of the phase diagrams between the weak-coupling theory [19, 33] and experiment [33, 40] strongly suggests an essential role of local inversion symmetry breaking in CeRh<sub>2</sub>As<sub>2</sub>, and the two superconducting phases were interpreted based on the even-odd parity transition within the superconducting state [33, 40].

In contrast to the preceding argument, there are two issues regarding the nature of CeRh<sub>2</sub>As<sub>2</sub>. First, the microscopic mechanism of superconductivity in CeRh<sub>2</sub>As<sub>2</sub> has been unsolved. The unconventional superconductiv-

ity mediated by quantum critical fluctuations is studied in this Letter. Second, the parity transition field of CeRh<sub>2</sub>As<sub>2</sub> significantly exceeds the Pauli-Clogston-Chandrasekhar limit and is larger than the prediction of weak-coupling theory by a factor of five [19, 33]. Although two scenarios have been proposed within the weak-coupling theory [44, 45], we try to resolve the issue by verifying an intrinsic phase diagram of strongly correlated locally noncentrosymmetric superconductors.

To tackle above mentioned problems, we focus on the electronic correlation effect of Ce  $f$ -electrons, which have localized character. Indeed, the large electronic specific heat coefficient  $\gamma \sim 1000$  mJ/mol K<sup>2</sup> supports the presence of heavy-fermion bands near the Fermi-level, and non-Fermi liquid behaviors suggest quantum criticality in CeRh<sub>2</sub>As<sub>2</sub> [33, 37, 39]. These experimental observations indicate that Coulomb interaction crucially impacts the electronic state of CeRh<sub>2</sub>As<sub>2</sub>. Hence, theoretical studies of strong correlation effects in locally noncentrosymmetric superconductors have been desired.

In this Letter, we conduct a thorough study on quantum critical multipole fluctuations, resulting superconductivity, and superconducting phase diagrams of locally noncentrosymmetric strongly correlated electron systems. To clarify these properties, fluctuation exchange (FLEX) approximation which appropriately reproduces critical behaviors of self-consistent renormalization theory [47] is adopted. In the FLEX scheme, the Green function and the self-energy depend on each other, and therefore, the retardation effect, quasi-particle scattering, and internal field are taken into account [48]. Theoretical results are compared with the superconducting phase diagrams of CeRh<sub>2</sub>As<sub>2</sub>, and the origin of superconductivity is discussed. As a result, the  $XY$ -type antiferromagnetic fluctuation consistent with the nuclear magnetic resonance (NMR) [39] and superconductivity with dominant  $d_{x^2-y^2}$ -wave pairing are revealed, and the obtained enhanced parity transition field resolves the issue of phase diagram in CeRh<sub>2</sub>As<sub>2</sub>.

*Bilayer Rashba-Hubbard model.* — We construct the bilayer Rashba-Hubbard model, in which Ce  $f$ -orbital,

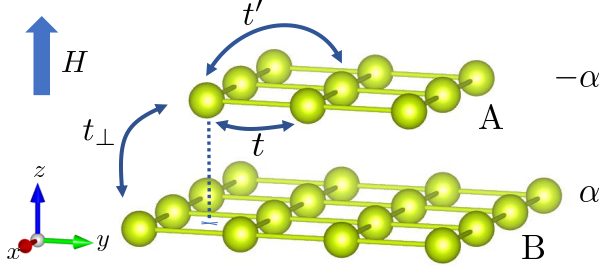


FIG. 1. Schematic figure of the bilayer Rashba-Hubbard model. Yellow circles represent the Ce atoms of CeRh<sub>2</sub>As<sub>2</sub>. We introduce first- and second-neighbor intra-layer hopping integrals. We also introduce an inter-layer hopping integral as  $t_{\perp}$ . The staggered Rashba-type antisymmetric spin-orbit coupling is included in the model as it arises from the asymmetric potential by Rh<sub>2</sub>As<sub>2</sub> layers. The magnetic field is applied parallel to the  $z$ -axis.

Coulomb correlation, and spin-orbit coupling are taken into account [49, 50]. The model is given by

$$\hat{H} = \sum_{\mathbf{k}} \varphi^{\dagger}(\mathbf{k}) \mathcal{H}_0(\mathbf{k}) \varphi(\mathbf{k}) + U \sum_{i,\sigma} n_{i\uparrow\sigma} n_{i\downarrow\sigma}, \quad (1)$$

where  $U$  is the on-site Coulomb repulsion,  $\mathcal{H}_0(\mathbf{k}) = \varepsilon(\mathbf{k})s_0 \otimes \sigma_0 + \alpha \mathbf{g}(\mathbf{k}) \cdot \mathbf{s} \otimes \sigma_z - \mu_B H s_z \otimes \sigma_0 + \tilde{t}_{\perp}(\mathbf{k})s_0 \otimes \sigma_+ + \tilde{t}_{\perp}(-\mathbf{k})s_0 \otimes \sigma_-$ ,  $\varphi(\mathbf{k}) = (c_{\mathbf{k}\uparrow A}, c_{\mathbf{k}\downarrow A}, c_{\mathbf{k}\uparrow B}, c_{\mathbf{k}\downarrow B})^{\top}$ , and  $c_{\mathbf{k}s\sigma}$  ( $c_{\mathbf{k}s\sigma}^{\dagger}$ ) is an annihilation (creation) operator for an electron with momentum  $\mathbf{k}$ , spin  $s$ , and sublattice  $\sigma \in \{A, B\}$  [Fig. 1]. Here,  $s_{\mu}$  and  $\sigma_{\mu}$  consisting of the  $2 \times 2$  unit matrix and three Pauli matrices represent spin and sublattice degrees of freedom, respectively.<sup>1</sup> The first term of  $\mathcal{H}_0$  represents intra-layer hopping including the chemical potential and is given by  $\varepsilon(\mathbf{k}) = -2t(\cos k_x + \cos k_y) + 4t' \cos k_x \cos k_y - \mu$ . The vector  $\mathbf{g}(\mathbf{k})$  describes the Rashba-type antisymmetric spin-orbit coupling given by  $\mathbf{g}(\mathbf{k}) = (-\partial\varepsilon(\mathbf{k})/\partial k_y, \partial\varepsilon(\mathbf{k})/\partial k_x, 0)$ , and  $H$  represents the Zeeman magnetic field parallel to the  $z$ -axis. The last two terms of  $\mathcal{H}_0$  describe inter-layer hopping given as  $\tilde{t}_{\perp}(\mathbf{k}) = t_{\perp}(1 + e^{-ik_x})(1 + e^{-ik_y})$ . This model is a straightforward extension of the Rashba-Hubbard model for globally inversion-asymmetric strongly correlated electron systems [51–63]. Hereafter, we set  $t' = 0.3$ ,  $t_{\perp} = 0.1$ ,  $\mu_B = 1$ , and  $U = 3.9$  with a unit of energy  $t = 1$  and determine the chemical potential so that the electron density per site  $n$  is 0.85.

*Multipole susceptibility.* — First, we discuss quantum critical multipole fluctuations. Dynamical susceptibility tensor is given by the generalized susceptibility as

$$\chi_{\hat{O}}(\mathbf{q}, i\nu_n) = \sum_{\xi_1 \xi_2 \xi_3 \xi_4} \hat{O}_{\xi_1 \xi_2} \chi_{\xi_2 \xi_1 \xi_3 \xi_4}(\mathbf{q}, i\nu_n) \hat{O}_{\xi_3 \xi_4}, \quad (2)$$

<sup>1</sup>  $\mu$  runs over  $\{0, x, y, z\}$ , and  $\sigma_{\pm}$  are given by  $(\sigma_x \pm i\sigma_y)/2$ .

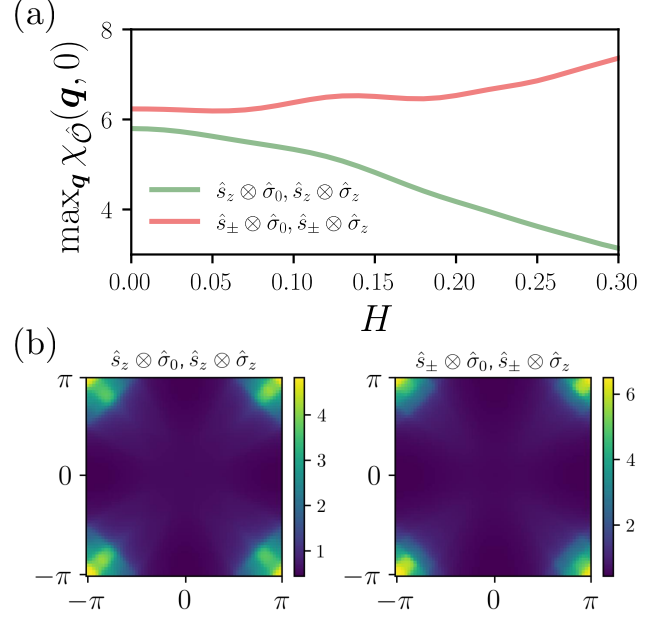


FIG. 2. (a) The magnetic field dependence of static multipole fluctuations. The maxima of the longitudinal and transverse magnetic susceptibilities are shown. Note that the even-parity and odd-parity multipole fluctuations are nearly degenerate. We assume  $\alpha/t_{\perp} = 2$  and  $T = 0.01$ . (b) The momentum dependence of longitudinal magnetic susceptibility (left) and transverse magnetic susceptibility (right) at  $H = 0.15$ .

where  $i\nu_n$  are bosonic Matsubara frequencies and  $\xi$  is abbreviated notation  $\xi = (s, \sigma)$ . The operators  $\hat{O}$  are (extended) multipole operators as  $\hat{O} = \hat{s} \otimes \hat{\sigma}$  [64–66], and classified into even-parity (odd-parity) multipole for  $\hat{\sigma}_0, \hat{\sigma}_x$  ( $\hat{\sigma}_y, \hat{\sigma}_z$ ). In Table I, we summarize the classification of multipole operators in our system. We adopt the normalization convention  $\text{tr}[\hat{O}^{\dagger} \hat{O}] = 1$ , and therefore, operators are represented by the Pauli matrices as  $\hat{s}_{\mu} = s_{\mu}/\sqrt{2}$  and  $\hat{\sigma}_{\mu} = \sigma_{\mu}/\sqrt{2}$ .

In Fig. 2(a), the magnetic field dependence of the maximum of transverse magnetic and longitudinal magnetic susceptibilities is shown. We see that the transverse (longitudinal) susceptibility is enhanced (reduced) by the magnetic field. Note that the even-parity magnetic multipole fluctuation for  $\mathbf{s} \otimes \sigma_0$  and the odd-parity magnetic multipole fluctuation for  $\mathbf{s} \otimes \sigma_z$  are nearly degenerate, while the odd-parity multipole is slightly favored. Other multipole susceptibilities are negligibly small. From Fig. 2(b), both transverse and longitudinal magnetic susceptibilities show the peak structure around  $\mathbf{Q} = (\pi, \pi)$ , and thus, the antiferromagnetic spin fluctuation develops in the system. The momentum dependence is not qualitatively affected by the magnetic field. Therefore, we conclude dominant  $XY$ -type antiferromagnetic fluctuation, which is consistent with the observation in CeRh<sub>2</sub>As<sub>2</sub> by the NMR measurement [39]. We confirmed

that the behaviors of the multipole susceptibility do not qualitatively depend on the strength of spin-orbit coupling  $\alpha/t_{\perp}$  [67].

TABLE I. The classification of the multipole operators in the bilayer Rashba-Hubbard model. Here,  $\hat{s}_{\pm} = (\hat{s}_x \pm i\hat{s}_y)/\sqrt{2}$  are ladder operators for spin. E (O) represents the even-parity (odd-parity) multipole operators. C, L, and T represent charge, longitudinal spin, and transverse spin operators respectively.  $\hat{\sigma}_0$  and  $\hat{\sigma}_z$  ( $\hat{\sigma}_x$  and  $\hat{\sigma}_y$ ) are intra-sublattice (inter-sublattice) operators.

$\hat{O}$	$\hat{\sigma}_0$	$\hat{\sigma}_x$	$\hat{\sigma}_y$	$\hat{\sigma}_z$
$\hat{s}_0$	E C intra	E C inter	O C intra	O C inter
$\hat{s}_z$	E L intra	E L inter	O L intra	O L inter
$\hat{s}_{\pm}$	E T intra	E T inter	O T intra	O T inter

*Superconductivity.* — The crystalline space group of  $\text{CeRh}_2\text{As}_2$  is  $P4/nmm$  (No.129), and therefore, the point group is  $D_{4h}$ . Since we introduce the magnetic field parallel to the  $z$ -axis, some symmetry operations are prohibited, and the point group reduces to  $C_{4h}$ . Hence, the superconducting gap functions are classified based on irreducible representations of  $C_{4h}$ . Using the conventional notation, we decompose the superconducting gap functions into the spin-singlet component and spin-triplet component,

$$\Delta^{\sigma\sigma'}(\mathbf{k}) = \{\psi^{\sigma\sigma'}(\mathbf{k}) + \mathbf{d}^{\sigma\sigma'}(\mathbf{k}) \cdot \mathbf{s}\}is_y, \quad (3)$$

for the intra-sublattice and inter-sublattice pairing channels. Here,  $\psi^{\text{AA}}(\mathbf{k})$  ( $\psi^{\text{AB}}(\mathbf{k})$ ) represents an intra-sublattice (inter-sublattice) spin-singlet order parameter, while  $\mathbf{d}^{\text{AA}}(\mathbf{k})$  ( $\mathbf{d}^{\text{AB}}(\mathbf{k})$ ) is an intra-sublattice (inter-sublattice) spin-triplet order parameter. In the following calculations, order parameters of inter-sublattice pairing are negligibly small. The basis functions of intra-sublattice order parameter for each irreducible representations of  $C_{4h}$  are summarized in Table II.

In Fig. 3(a), the eigenvalues of Éliashberg equation for each irreducible representation are shown [68]. The  $B_g$  and  $B_u$  representations are dominant. From the momentum dependence displayed in Fig. 3(b), both of these states contain spin-singlet  $d_{x^2-y^2}$ -wave dominant pairing as well as spin-triplet subdominant pairing with  $p$ -wave symmetry. These unconventional Cooper pairs are stabilized by the antiferromagnetic fluctuations and spin-orbit coupling and not significantly changed against the magnetic field.

While almost the same momentum dependence, the different sublattice structures of gap functions distinguish the  $B_g$  and  $B_u$  representations. In the even-parity  $B_g$  representation, the spin-singlet (spin-triplet) gap function has the same (opposite) sign between the sublattices A and B, as  $\psi^{\text{AA}}(\mathbf{k}) = \psi^{\text{BB}}(\mathbf{k})$  and  $\mathbf{d}^{\text{AA}}(\mathbf{k}) = -\mathbf{d}^{\text{BB}}(\mathbf{k})$ . On the other hand,  $\psi^{\text{AA}}(\mathbf{k}) = -\psi^{\text{BB}}(\mathbf{k})$  and  $\mathbf{d}^{\text{AA}}(\mathbf{k}) = \mathbf{d}^{\text{BB}}(\mathbf{k})$  in the odd-parity  $B_u$  representation.

Therefore, the  $B_g$  and  $B_u$  representations correspond to the BCS and PDW states predicted in the weak-coupling theory [19]. As shown in Fig 3(a), eigenvalues of the Éliashberg equation for both  $B_g$  and  $B_u$  representations are weakened by the magnetic field due to the Pauli depairing effect. However, the  $B_u$  state is more robust compared with the  $B_g$  state, and therefore, at  $H = 0.24$  the parity transition from the even-parity  $B_g$  state to the odd-parity  $B_u$  state occurs. The transition can be understood from the viewpoint of the intrinsic magnetic response of these states. Indeed, the  $B_g$  state is Pauli-limited, but the  $B_u$  state mostly avoids the Pauli limiting because the magnetic susceptibility does not decrease through the superconducting transition [18, 30].

TABLE II. The basis functions for intra-sublattice superconducting order parameter. IR represents the irreducible representations of the point group  $C_{4h}$ . We take into account the time-reversal symmetry breaking under the magnetic field, and the degeneracy of the  $E_{g/u}$  states is lifted. Thus, we distinguish them as  $E_{g/u}^1$  and  $E_{g/u}^2$ . Note that the spin-singlet component  $\psi(\mathbf{k})$  and spin-triplet in-plane component  $d_{x,y}(\mathbf{k})$  for the  $E$  representations are prohibited due to the  $C_2^z$  rotation symmetry.

IR	$\psi(\mathbf{k})$	$\mathbf{d}(\mathbf{k})$
$A_g, A_u$	$1, k_x k_y (k_x^2 - k_y^2)$	$k_x \hat{x} + k_y \hat{y}, k_y \hat{x} - k_x \hat{y}$
$B_g, B_u$	$k_x k_y, k_x^2 - k_y^2$	$k_x \hat{x} - k_y \hat{y}, k_y \hat{x} + k_x \hat{y}$
$E_g^1, E_u^1$	0	$(k_x + ik_y) \hat{z}$
$E_g^2, E_u^2$	0	$(k_x - ik_y) \hat{z}$

*Phase diagram.* — Let us discuss the  $H$ - $T$  phase diagram of the bilayer Rashba-Hubbard model. In Figs. 4(a)-(d), we show the phase diagrams for  $\alpha/t_{\perp} = 0, 1, 2,$  and  $3$ , which is known as a control parameter of local noncentrosymmetry [18].<sup>2</sup> We show the superconducting transition lines [69] of the  $B_g$  and  $B_u$  states, which correspond to the BCS and PDW states as mentioned before.

From the obtained phase diagrams, the zero-field superconducting transition temperature  $T_c$  and the magnetic field at the parity transition point  $H^*$  are estimated as  $(T_c, H^*) = (0.0141, 0.195), (0.0135, 0.212),$  and  $(0.0124, 0.192)$  for  $\alpha/t_{\perp} = 1, 2,$  and  $3$ , respectively. From these estimations, we evaluate  $H^*$  with a unit of  $T_c$ ,

$$\frac{H^*}{T_c} = \begin{cases} 13.8 & (\alpha/t_{\perp} = 1) \\ 15.7 & (\alpha/t_{\perp} = 2) \\ 15.5 & (\alpha/t_{\perp} = 3). \end{cases} \quad (4)$$

<sup>2</sup> While the case  $\alpha/t_{\perp} = 0$  corresponds to the bilayer system without spin-orbit coupling, for  $\alpha/t_{\perp} = \infty$  the system is equivalent to a set of monolayer systems with Rashba-type spin-orbit coupling [18].

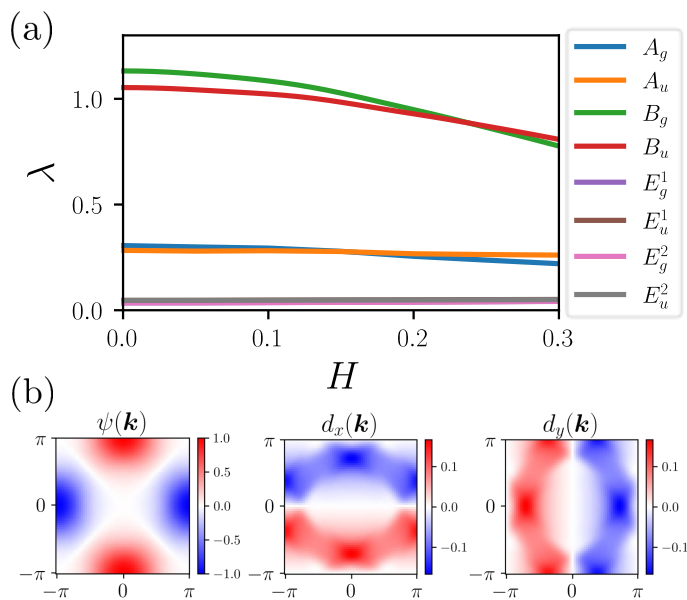


FIG. 3. (a) The magnetic field dependence of eigenvalues of the Éliashberg equation for each irreducible representation. We assume  $\alpha/t_{\perp} = 2$  and  $T = 0.01$ . (b) The momentum dependence of intra-sublattice spin-singlet and spin-triplet gap functions,  $\psi^{\text{AA}}(\mathbf{k})$  and  $\mathbf{d}^{\text{AA}}(\mathbf{k})$ , of the  $B_g$  representation for  $H = 0.15$ . Note that  $d_z^{\sigma\sigma}(\mathbf{k}) = 0$ . Results for the  $B_u$  representation are almost the same as the figures.

Thus, we conclude that the parity transition fields scaled by transition temperature are approximately  $H^*/T_c \simeq 15$  and universal against variation of  $\alpha/t_{\perp}$ . Although a much smaller value  $H^*/T_c \simeq 2$  was predicted by the mean-field theory [19], in  $\text{CeRh}_2\text{As}_2$  experimental values  $H^* \simeq 3.9$  T and  $T_c \simeq 0.26$  K lead  $(H^*/T_c)_{\text{exp}} \simeq 10$  [33]. Hence, our theoretical result is quantitatively consistent with the phase diagram of  $\text{CeRh}_2\text{As}_2$  and resolves the discrepancy between the weak-coupling theory and experiment.

Now we discuss the origin of the enhancement in the parity transition field  $H^*$ . First, a possible origin is the nonsymmorphic crystalline symmetry as proposed in Ref. 45. Actually, an indicator of local noncentrosymmetry  $\alpha/\hat{t}_{\perp}(\mathbf{k})$  diverges at the Brillouin Zone faces in nonsymmorphic crystals because of  $\hat{t}_{\perp}(\mathbf{k}_{\text{face}}) = 0$ , and therefore, the effect of the spin-orbit coupling is more essential than the symmorphic case [45, 70]. However, our analysis of the bilayer Rashba-Hubbard model does not support this possibility, because the ratio  $H^*/T_c$  is universal against variation of  $\alpha/t_{\perp}$ . Second, we may expect that the spin-triplet component in the gap function changes the spin state of Cooper pairs and increases  $H^*$ . However, this is also unlikely because we observe strong dependence on  $\alpha/t_{\perp}$  of the parity mixing parameter  $r$

(Fig. 5), which is defined as

$$r = \frac{\max_{\mathbf{k}} |\mathbf{d}^{\text{AA}}(\mathbf{k})|^2}{\max_{\mathbf{k}} |\psi^{\text{AA}}(\mathbf{k})|^2}. \quad (5)$$

From Eq. (4) and Fig. 5, we find that  $H^*/T_c$  and  $r$  are almost uncorrelated. Third, we rule out the field dependence of effective interaction as the main origin. In the bilayer Rashba-Hubbard model, the effective pairing interaction is field-dependent because of the field-enhanced magnetic anisotropy (see Fig. 2). Figure 6 shows eigenvalues of the Éliashberg equation with and without the field dependence of magnetic anisotropy,<sup>3</sup> and we find that the field-enhanced magnetic anisotropy weakens the superconducting instabilities. However, the parity transition field  $H^*$  is hardly affected. Thus, the field-enhanced magnetic anisotropy is also irrelevant for the enhancement of  $H^*$ . We conclude from these considerations that a large parity transition field consistent with  $\text{CeRh}_2\text{As}_2$  is due to the internal field arising from the quantum critical antiferromagnetic fluctuation. Near the antiferromagnetic critical point, the spin correlation significantly screens the Zeeman field and increases the scale of magnetic fields [71]. This is consistent with the large upper critical fields of  $\text{CeRh}_2\text{As}_2$  which significantly exceeds the Pauli-Clogston-Chandrasekhar limit even for the in-plane direction [33].

*Conclusion.* — We investigated the nature of quantum critical multipole fluctuation and superconductivity in the bilayer Rashba-Hubbard model, a minimal model of locally noncentrosymmetric strongly correlated electron systems. Experimental observations in a recently discovered superconductor  $\text{CeRh}_2\text{As}_2$  [33] were discussed. The  $XY$ -type antiferromagnetic fluctuations are shown consistent with the NMR study [39], and the applied magnetic field along the  $z$ -axis enhances the fluctuations. Due to the critical antiferromagnetic fluctuation, superconductivity with dominant  $d_{x^2-y^2}$ -wave pairing and subdominant  $p$ -wave pairing is stabilized, and the two superconducting phases with different space inversion parity appear in the  $H$ - $T$  phase diagram, consistent with  $\text{CeRh}_2\text{As}_2$ . The parity transition field is enhanced by the quantum critical fluctuation, and the obtained value is in quantitative agreement with the experimental value. These results support the parity transition in the superconducting state of  $\text{CeRh}_2\text{As}_2$  [33] and indicate the topological superconductivity [32]. Our theory not only solves the issues of  $\text{CeRh}_2\text{As}_2$  but also elucidates general behaviors of the family of locally noncentrosymmetric strongly correlated superconductors.

The authors are grateful to A. Daido and S. Sumita for fruitful discussions. Some figures in this work were

<sup>3</sup> To investigate the effect of the field-induced change of effective interaction, we solve the Éliashberg equation with the zero-field vertex functions while the Green functions at  $H \neq 0$  are adopted.

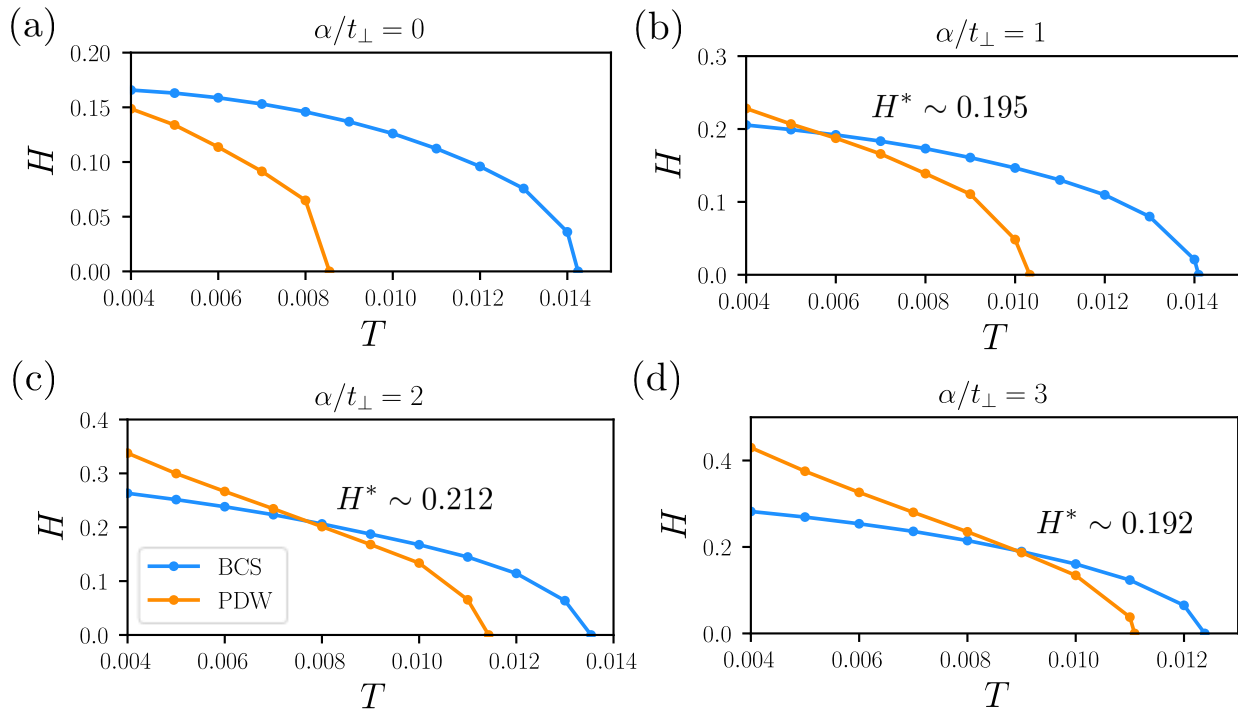


FIG. 4. (a)-(d)  $H$ - $T$  phase diagrams of the bilayer Rashba-Hubbard model for  $\alpha/t_{\perp} = 0, 1, 2, 3$ . We show the superconducting transition lines of the even-parity  $B_g$  and odd-parity  $B_u$  states, on which eigenvalues of the Éliashberg equation become unity. The BCS and PDW states correspond to the  $B_g$  and  $B_u$  superconducting phases, respectively.  $H^*$  denotes the magnetic field at the parity transition point.

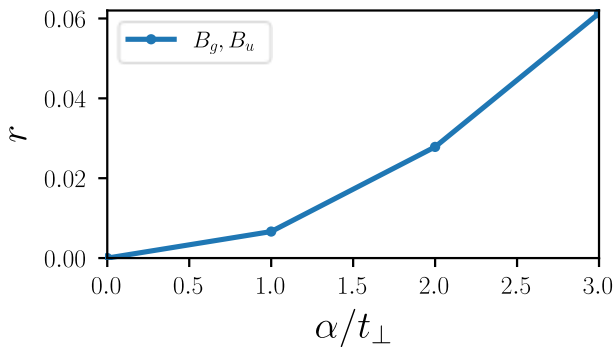


FIG. 5. The parity mixing parameter  $r$  as a function of  $\alpha/t_{\perp}$ . The values for the  $B_g$  and  $B_u$  representations are nearly the same. We assume  $T = 0.01$  and  $H = 0.15$ .

created by using VESTA [72]. This work was supported by JSPS KAKENHI (Grants Nos. JP18H01178, JP18H05227, JP20H05159, JP21J23007, JP21K18145, JP22H01181) and SPIRITS 2020 of Kyoto University.

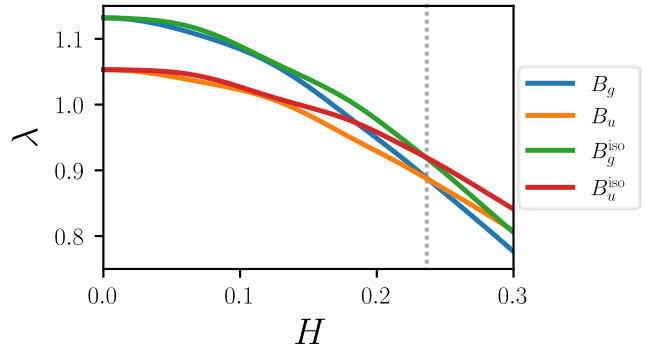


FIG. 6. The magnetic field dependence of eigenvalues of the Éliashberg equation for the  $B_g$  and  $B_u$  representations.  $B_g^{\text{iso}}$  and  $B_u^{\text{iso}}$  represent the eigenvalues without the field-enhanced magnetic anisotropy. The parity transition points are indicated by the gray dashed line. We assume  $\alpha/t_{\perp} = 2$  and  $T = 0.01$ .

- [1] Xiao-Liang Qi and Shou-Cheng Zhang, “Topological insulators and superconductors,” *Rev. Mod. Phys.* **83**, 1057–1110 (2011).
- [2] Yukio Tanaka, Masatoshi Sato, and Naoto Nagaosa, “Symmetry and topology in superconductors –odd-frequency pairing and edge states–,” *Journal of the Phys-*

\* [nogaki.kosuke.83v@st.kyoto-u.ac.jp](mailto:nogaki.kosuke.83v@st.kyoto-u.ac.jp)



- ical Society of Japan **81**, 011013 (2012).
- [3] Masatoshi Sato and Satoshi Fujimoto, “Majorana fermions and topology in superconductors,” *Journal of the Physical Society of Japan* **85**, 072001 (2016).
- [4] Masatoshi Sato and Yoichi Ando, “Topological superconductors: a review,” *Reports on Progress in Physics* **80**, 076501 (2017).
- [5] J. Bardeen, L. N. Cooper, and J. R. Schrieffer, “Theory of superconductivity,” *Phys. Rev.* **108**, 1175–1204 (1957).
- [6] Robert Joynt and Louis Taillefer, “The superconducting phases of  $uPt_3$ ,” *Rev. Mod. Phys.* **74**, 235–294 (2002).
- [7] Yasumasa Tsutsumi, Masaki Ishikawa, Takuto Kawakami, Takeshi Mizushima, Masatoshi Sato, Masanori Ichioka, and Kazushige Machida, “ $Upt_3$  as a topological crystalline superconductor,” *Journal of the Physical Society of Japan* **82**, 113707 (2013).
- [8] Youichi Yanase, “Nonsymmorphic weyl superconductivity in  $uPt_3$  based on  $E_{2u}$  representation,” *Phys. Rev. B* **94**, 174502 (2016).
- [9] Youichi Yanase and Ken Shiozaki, “Möbius topological superconductivity in  $uPt_3$ ,” *Phys. Rev. B* **95**, 224514 (2017).
- [10] Dai Aoki and Jacques Flouquet, “Superconductivity and ferromagnetic quantum criticality in uranium compounds,” *Journal of the Physical Society of Japan* **83**, 061011 (2014).
- [11] Dai Aoki, Kenji Ishida, and Jacques Flouquet, “Review of  $u$ -based ferromagnetic superconductors: Comparison between  $uGe_2$ ,  $uRh_2$ , and  $uCoGe$ ,” *Journal of the Physical Society of Japan* **88**, 022001 (2019).
- [12] Akito Daido, Tsuneya Yoshida, and Youichi Yanase, “ $F_4$  topological superconductivity in  $uCoGe$ ,” *Phys. Rev. Lett.* **122**, 227001 (2019).
- [13] Jun Ishizuka, Shuntaro Sumita, Akito Daido, and Youichi Yanase, “Insulator-metal transition and topological superconductivity in  $uTe_2$  from a first-principles calculation,” *Phys. Rev. Lett.* **123**, 217001 (2019).
- [14] Jun Ishizuka and Youichi Yanase, “Periodic anderson model for magnetism and superconductivity in  $uTe_2$ ,” *Phys. Rev. B* **103**, 094504 (2021).
- [15] Dai Aoki, Jean-Pascal Brison, Jacques Flouquet, Kenji Ishida, Georg Knebel, Y. Tokunaga, and Youichi Yanase, “Unconventional superconductivity in  $uTe_2$ ,” *Journal of Physics: Condensed Matter* (2022).
- [16] Hiroki Fujibayashi, Genki Nakamine, Katsuki Kinjo, Shunsaku Kitagawa, Kenji Ishida, Yo Tokunaga, Hironori Sakai, Shinsaku Kambe, Ai Nakamura, Yusei Shimizu, Yoshiya Homma, Dexin Li, Fuminori Honda, and Dai Aoki, “Superconducting order parameter in  $uTe_2$  determined by knight shift measurement,” *Journal of the Physical Society of Japan* **91**, 043705 (2022).
- [17] Mark H. Fischer, Florian Loder, and Manfred Sigrist, “Superconductivity and local noncentrosymmetry in crystal lattices,” *Phys. Rev. B* **84**, 184533 (2011).
- [18] Daisuke Maruyama, Manfred Sigrist, and Youichi Yanase, “Locally non-centrosymmetric superconductivity in multilayer systems,” *Journal of the Physical Society of Japan* **81**, 034702 (2012).
- [19] Tomohiro Yoshida, Manfred Sigrist, and Youichi Yanase, “Pair-density wave states through spin-orbit coupling in multilayer superconductors,” *Phys. Rev. B* **86**, 134514 (2012).
- [20] Tomohiro Yoshida, Manfred Sigrist, and Youichi Yanase, “Complex-stripe phases induced by staggered rashba spin-orbit coupling,” *Journal of the Physical Society of Japan* **82**, 074714 (2013).
- [21] Tomohiro Yoshida, Manfred Sigrist, and Youichi Yanase, “Parity-mixed superconductivity in locally non-centrosymmetric system,” *Journal of the Physical Society of Japan* **83**, 013703 (2014).
- [22] Tomohiro Yoshida, Manfred Sigrist, and Youichi Yanase, “Topological crystalline superconductivity in locally noncentrosymmetric multilayer superconductors,” *Phys. Rev. Lett.* **115**, 027001 (2015).
- [23] Yoichi Higashi, Yuki Nagai, Tomohiro Yoshida, Yusuke Masaki, and Youichi Yanase, “Robust zero-energy bound states around a pair-density-wave vortex core in locally noncentrosymmetric superconductors,” *Phys. Rev. B* **93**, 104529 (2016).
- [24] Masaaki Shimozaawa, Swee K Goh, Takasada Shibauchi, and Yuji Matsuda, “From kondo lattices to kondo superlattices,” *Reports on Progress in Physics* **79**, 074503 (2016).
- [25] Shi-Long Wu, Kazuki Sumida, Koji Miyamoto, Kazuaki Taguchi, Tomoki Yoshikawa, Akio Kimura, Yoshifumi Ueda, Masashi Arita, Masanori Nagao, Satoshi Watauchi, Isao Tanaka, and Taichi Okuda, “Direct evidence of hidden local spin polarization in a centrosymmetric superconductor  $LaO_{0.55}F_{0.45}Bi_2$ ,” *Nature Communications* **8**, 1919 (2017).
- [26] Tsuneya Yoshida, Akito Daido, Youichi Yanase, and Norio Kawakami, “Fate of majorana modes in  $CeCoIn_5/YbCoIn_5$  superlattices: A test bed for the reduction of topological classification,” *Phys. Rev. Lett.* **118**, 147001 (2017).
- [27] Yasuharu Nakamura and Youichi Yanase, “Odd-parity superconductivity in bilayer transition metal dichalcogenides,” *Phys. Rev. B* **96**, 054501 (2017).
- [28] Kenneth Gotlieb, Chiu-Yun Lin, Maksym Serbyn, Wentao Zhang, Christopher L. Smallwood, Christopher Jozwiak, Hiroshi Eisaki, Zahid Hussain, Ashvin Vishwanath, and Alessandra Lanzara, “Revealing hidden spin-momentum locking in a high-temperature cuprate superconductor,” *Science* **362**, 1271–1275 (2018).
- [29] David Möckli, Youichi Yanase, and Manfred Sigrist, “Orbitally limited pair-density-wave phase of multilayer superconductors,” *Phys. Rev. B* **97**, 144508 (2018).
- [30] Anastasiia Skurativska, Manfred Sigrist, and Mark H. Fischer, “Spin response and topology of a staggered-rashba superconductor,” *Phys. Rev. Research* **3**, 033133 (2021).
- [31] Mark H Fischer, Manfred Sigrist, Daniel F Agterberg, and Youichi Yanase, “Superconductivity and local inversion-symmetry breaking,” (2022).
- [32] Kosuke Nogaki, Akito Daido, Jun Ishizuka, and Youichi Yanase, “Topological crystalline superconductivity in locally noncentrosymmetric  $CeRh_2As_2$ ,” *Phys. Rev. Research* **3**, L032071 (2021).
- [33] S. Khim, J. F. Landaeta, J. Banda, N. Bannor, M. Brando, P. M. R. Brydon, D. Hafner, R. Kuchler, R. Cardoso-Gil, U. Stockert, A. P. Mackenzie, D. F. Agterberg, C. Geibel, and E. Hassinger, “Field-induced transition within the superconducting state of  $CeRh_2As_2$ ,” *Science* **373**, 1012–1016 (2021).
- [34] Alexandre Poret and Georg Knebel, “Driving multiphase superconductivity,” *Science* **373**, 962–963 (2021).
- [35] Shin-ichi Kimura, Jörg Sichelschmidt, and Seunghyun Khim, “Optical study of the electronic structure of  $LaO_{0.55}F_{0.45}Bi_2$ ,” *Journal of the Physical Society of Japan* **82**, 074714 (2013).

- cally noncentrosymmetric  $\text{CeRh}_2\text{As}_2$ ,” *Phys. Rev. B* **104**, 245116 (2021).
- [36] Seita Onishi, Ulrike Stockert, Seunghyun Khim, Jacintha Banda, Manuel Brando, and Elena Hassinger, “Low-temperature thermal conductivity of the two-phase superconductor  $\text{cerh}_2\text{as}_2$ ,” *Frontiers in Electronic Materials* **2** (2022), 10.3389/femat.2022.880579.
- [37] D. Hafner, P. Khanenko, E.-O. Eljaouhari, R. Kuchler, J. Banda, N. Bannor, T. Lühmann, J. F. Landaeta, S. Mishra, I. Sheikin, E. Hassinger, S. Khim, C. Geibel, G. Zwirnagl, and M. Brando, “Possible quadrupole density wave in the superconducting kondo lattice  $\text{cerh}_2\text{as}_2$ ,” *Phys. Rev. X* **12**, 011023 (2022).
- [38] Mayu Kibune, Shunsaku Kitagawa, Katsuki Kinjo, Shiki Ogata, Masahiro Manago, Takanori Taniguchi, Kenji Ishida, Manuel Brando, Elena Hassinger, Helge Rosner, Christoph Geibel, and Seunghyun Khim, “Observation of antiferromagnetic order as odd-parity multipoles inside the superconducting phase in  $\text{cerh}_2\text{as}_2$ ,” *Phys. Rev. Lett.* **128**, 057002 (2022).
- [39] Shunsaku Kitagawa, Mayu Kibune, Katsuki Kinjo, Masahiro Manago, Takanori Taniguchi, Kenji Ishida, Manuel Brando, Elena Hassinger, Christoph Geibel, and Seunghyun Khim, “Two-dimensional xy-type magnetic properties of locally noncentrosymmetric superconductor  $\text{cerh}_2\text{as}_2$ ,” *Journal of the Physical Society of Japan* **91**, 043702 (2022).
- [40] J. F. Landaeta, P. Khanenko, D. C. Cavanagh, C. Geibel, S. Khim, S. Mishra, I. Sheikin, P. M. R. Brydon, D. F. Agterberg, M. Brando, and E. Hassinger, “Field-angle dependence reveals odd-parity superconductivity in  $\text{cerh}_2\text{as}_2$ ,” (2022).
- [41] Eric G. Schertenleib, Mark H. Fischer, and Manfred Sigrist, “Unusual  $h-t$  phase diagram of  $\text{CeRh}_2\text{As}_2$ : The role of staggered noncentrosymmetry,” *Phys. Rev. Research* **3**, 023179 (2021).
- [42] David Möckli and Aline Ramires, “Two scenarios for superconductivity in  $\text{cerh}_2\text{as}_2$ ,” *Phys. Rev. Research* **3**, 023204 (2021).
- [43] Andrzej Ptak, Konrad J. Kapcia, Paweł T. Jochym, Jan Łażewski, Andrzej M. Oleś, and Przemysław Piekarczyk, “Electronic and dynamical properties of  $\text{cerh}_2\text{as}_2$ : Role of  $\text{rh}_2\text{as}_2$  layers and expected orbital order,” *Phys. Rev. B* **104**, L041109 (2021).
- [44] David Möckli and Aline Ramires, “Superconductivity in disordered locally noncentrosymmetric materials: An application to  $\text{cerh}_2\text{as}_2$ ,” *Phys. Rev. B* **104**, 134517 (2021).
- [45] D. C. Cavanagh, T. Shishidou, M. Weinert, P. M. R. Brydon, and Daniel F. Agterberg, “Nonsymmorphic symmetry and field-driven odd-parity pairing in  $\text{CeRh}_2\text{As}_2$ ,” *Phys. Rev. B* **105**, L020505 (2022).
- [46] Tamaghna Hazra and Piers Coleman, “Triplet pairing mechanisms from hund’s-kondo models: applications to  $\text{ute}_2$  and  $\text{cerh}_2\text{as}_2$ ,” (2022).
- [47] Tôru Moriya and Kazuo Ueda, “Spin fluctuations and high temperature superconductivity,” *Advances in Physics* **49**, 555–606 (2000).
- [48] See Supplemental Material at [URL will be inserted by publisher] for detailed description of FLEX approximation [See Sec. S1].
- [49] L. Craco, “Correlated nature of hybrid  $s$ -wave superconducting and rashba lattices,” *Phys. Rev. B* **104**, 064509 (2021).
- [50] Xiancong Lu and D. Sénéchal, “Spin texture in a bilayer high-temperature cuprate superconductor,” *Phys. Rev. B* **104**, 024502 (2021).
- [51] Ernst Bauer and Manfred Sigrist, *Non-centrosymmetric superconductors: introduction and overview*, Vol. 847 (Springer Science & Business Media, 2012).
- [52] Keisuke Shigeta, Seichiro Onari, and Yukio Tanaka, “Superconducting pairing symmetry on the extended hubbard model in the presence of the rashba-type spin-orbit coupling,” *Journal of the Physical Society of Japan* **82**, 014702 (2013).
- [53] Yukinobu Fujimoto, Kazumasa Miyake, and Hiroyasu Matsuura, “Deformation of the fermi surface and anomalous mass renormalization by critical spin fluctuations through asymmetric spin-orbit interaction,” *Journal of the Physical Society of Japan* **84**, 043702 (2015).
- [54] Daisuke Maruyama and Youichi Yanase, “Electron correlation effects in non-centrosymmetric metals in the weak coupling regime,” *Journal of the Physical Society of Japan* **84**, 074702 (2015).
- [55] Andrés Greco and Andreas P. Schnyder, “Mechanism for unconventional superconductivity in the hole-doped rashba-hubbard model,” *Phys. Rev. Lett.* **120**, 177002 (2018).
- [56] Xiancong Lu and D. Sénéchal, “Parity-mixing superconducting phase in the rashba-hubbard model and its topological properties from dynamical mean-field theory,” *Phys. Rev. B* **98**, 245118 (2018).
- [57] Rasoul Ghadimi, Mehdi Kargarian, and S. Akbar Jafari, “Competing superconducting phases in the interacting two-dimensional electron gas with strong rashba spin-orbit coupling,” *Phys. Rev. B* **99**, 115122 (2019).
- [58] Andrés Greco, Matías Bejas, and Andreas P. Schnyder, “Ferromagnetic fluctuations in the rashba-hubbard model,” *Phys. Rev. B* **101**, 174420 (2020).
- [59] Kosuke Nogaki and Youichi Yanase, “Strongly parity-mixed superconductivity in the rashba-hubbard model,” *Phys. Rev. B* **102**, 165114 (2020).
- [60] Sebastian Wolf and Stephan Rachel, “Spin-orbit coupled superconductivity: Rashba-hubbard model on the square lattice,” *Phys. Rev. B* **102**, 174512 (2020).
- [61] Matthew J. Trott and Chris A. Hooley, “Mixed-parity superconductivity near lifshitz transitions in strongly spin-orbit-coupled metals,” *Phys. Rev. Research* **2**, 013106 (2020).
- [62] Rahul Soni, Amit Bikram Sanyal, Nitin Kaushal, Satoshi Okamoto, Adriana Moreo, and Elbio Dagotto, “Multitude of topological phase transitions in bipartite dice and lieb lattices with interacting electrons and rashba coupling,” *Phys. Rev. B* **104**, 235115 (2021).
- [63] Mehdi Biderang, Mohammad-Hossein Zare, and Jesko Sirker, “Proximity-driven ferromagnetism and superconductivity in the triangular rashba-hubbard model,” *Phys. Rev. B* **105**, 064504 (2022).
- [64] Hikaru Watanabe and Youichi Yanase, “Group-theoretical classification of multipole order: Emergent responses and candidate materials,” *Phys. Rev. B* **98**, 245129 (2018).
- [65] Satoru Hayami, Megumi Yatsushiro, Yuki Yanagi, and Hiroaki Kusunose, “Classification of atomic-scale multipoles under crystallographic point groups and application to linear response tensors,” *Phys. Rev. B* **98**, 165110 (2018).
- [66] Megumi Yatsushiro, Hiroaki Kusunose, and Satoru Hayami, “Multipole classification in 122 magnetic point

- groups for unified understanding of multiferroic responses and transport phenomena,” [Phys. Rev. B \*\*104\*\*, 054412 \(2021\)](#).
- [67] See Supplemental Material at [URL will be inserted by publisher] for the multipole susceptibility for different  $\alpha/t_{\perp}$  [See Sec. S3].
- [68] See Supplemental Material at [URL will be inserted by publisher] for the eigenvalues of Éliashberg equation for different  $\alpha/t_{\perp}$  [See Secs. S4 and S5].
- [69] See Supplemental Material at [URL will be inserted by publisher] for detailed description of Éliashberg equation [See Sec. S2].
- [70] Shuntaro Sumita and Youichi Yanase, “Superconductivity in magnetic multipole states,” [Phys. Rev. B \*\*93\*\*, 224507 \(2016\)](#).
- [71] Youichi Yanase, “Fflo superconductivity near the antiferromagnetic quantum critical point,” [Journal of the Physical Society of Japan \*\*77\*\*, 063705 \(2008\)](#).
- [72] Koichi Momma and Fujio Izumi, “*VESTA3* for three-dimensional visualization of crystal, volumetric and morphology data,” [Journal of Applied Crystallography \*\*44\*\*, 1272–1276 \(2011\)](#).



Supplemental Materials:  
**Even-odd parity transition in strongly correlated locally noncentrosymmetric  
 superconductors : An application to CeRh<sub>2</sub>As<sub>2</sub>**

**S1. SELF-CONSISTENT CONDITION FOR FLUCTUATION EXCHANGE APPROXIMATION**

The noninteracting Green functions for  $U = 0$  are expressed by the  $4 \times 4$  matrix form in the spin and sublattice basis,

$$G^{(0)}(\mathbf{k}, i\omega_n) = (i\omega_n s_0 \otimes \sigma_0 - \mathcal{H}_0(\mathbf{k}))^{-1}, \quad (\text{S1})$$

where  $\omega_n = (2n + 1)\pi T$  are fermionic Matsubara frequencies. In the interacting case  $U \neq 0$ , the dressed Green functions contain a self-energy,  $\Sigma(\mathbf{k}, i\omega_n)$ ,

$$G(\mathbf{k}, i\omega_n) = (i\omega_n s_0 \otimes \sigma_0 - \mathcal{H}_0(\mathbf{k}) - \Sigma(\mathbf{k}, i\omega_n))^{-1}. \quad (\text{S2})$$

Within the FLEX approximation, the self-energy is expressed with use of an effective interaction,  $\Gamma^n(\mathbf{k}, i\nu_n)$ , as

$$\Sigma_{\xi\xi'}(\mathbf{k}, i\omega_n) = \frac{T}{N} \sum_{\mathbf{q}, i\nu_n} \Gamma_{\xi\xi_1\xi'\xi_2}^n(\mathbf{q}, i\nu_n) G_{\xi_1\xi_2}(\mathbf{k} - \mathbf{q}, i\omega_n - i\nu_n), \quad (\text{S3})$$

and the effective interaction is given by

$$\Gamma_{\xi_1\xi_2\xi_3\xi_4}^n(\mathbf{k}, i\nu_n) = U_{\xi_1\xi_2\xi_3\xi_4} \left( \chi_{\xi_5\xi_6\xi_7\xi_8}(\mathbf{k}, i\nu_n) - \frac{1}{2} \chi_{\xi_5\xi_6\xi_7\xi_8}^{(0)}(\mathbf{k}, i\nu_n) \right) U_{\xi_7\xi_8\xi_3\xi_4}, \quad (\text{S4})$$

where  $U_{\xi_1\xi_2\xi_3\xi_4}$  is bare interaction tensor which satisfies the following relation

$$\sum_{\xi_1\xi_2\xi_3\xi_4} U_{\xi_1\xi_2\xi_3\xi_4} c_{\xi_1}^\dagger c_{\xi_2} c_{\xi_3} c_{\xi_4}^\dagger = U \sum_{i,\sigma} n_{i\uparrow\sigma} n_{i\downarrow\sigma}, \quad (\text{S5})$$

$$U_{\xi_1\xi_2\xi_3\xi_4} = \delta_{\sigma_1,\sigma_2} \delta_{\sigma_2,\sigma_3} \delta_{\sigma_3,\sigma_4} U_{s_1 s_2 s_3 s_4}, \quad (\text{S6})$$

$$U_{\uparrow\downarrow\uparrow\downarrow} = U_{\downarrow\uparrow\downarrow\uparrow} = -U_{\uparrow\uparrow\downarrow\downarrow} = -U_{\downarrow\downarrow\uparrow\uparrow} = U, \quad (\text{S7})$$

and  $i\nu_n$  are bosonic Matsubara frequencies. Here,  $\chi(\mathbf{k}, i\nu_n)$  is the generalized susceptibility. We introduce the bare susceptibility

$$\chi_{\xi_1\xi_2\xi_3\xi_4}^{(0)}(\mathbf{q}, i\nu_n) = -\frac{T}{N} \sum_{\mathbf{k}, i\omega_n} G_{\xi_1\xi_3}(\mathbf{k}, i\omega_n) G_{\xi_4\xi_2}(\mathbf{k} - \mathbf{q}, i\omega_n - i\nu_n), \quad (\text{S8})$$

and compute the generalized susceptibility by

$$\chi_{\xi_1\xi_2\xi_3\xi_4}(\mathbf{q}, i\nu_n) = \chi_{\xi_1\xi_2\xi_3\xi_4}^{(0)}(\mathbf{q}, i\nu_n) + \chi_{\xi_1\xi_2\xi_5\xi_6}^{(0)}(\mathbf{q}, i\nu_n) U_{\xi_5\xi_6\xi_7\xi_8} \chi_{\xi_7\xi_8\xi_3\xi_4}(\mathbf{q}, i\nu_n). \quad (\text{S9})$$

According to Eqs. (S2)-(S9),  $G$ ,  $\Sigma$ ,  $\Gamma^n$ ,  $\chi^{(0)}$ , and  $\chi$  depend on each other, and therefore, we self-consistently determine these functions.

For functions with fermionic Matsubara frequencies  $A(\mathbf{q}, i\omega_n)$ , the static limit  $A(\mathbf{q}, 0)$  is evaluated by an approximation justified at low temperatures,

$$A(\mathbf{q}, 0) \simeq \frac{A(\mathbf{q}, i\pi T) + A(\mathbf{q}, -i\pi T)}{2}. \quad (\text{S10})$$

**S2. LINEARIZED ÉLIASHBERG EQUATION**

To investigate superconductivity, we numerically solve the linearized Éliashberg equation which is given by

$$\lambda \Delta_{\xi\xi'}(k) = \frac{T}{N} \sum_{k'} \Gamma_{\xi\xi_1\xi_2\xi'}^a(k - k') G_{\xi_1\xi_3}(k') \Delta_{\xi_3\xi_4}(k') G_{\xi_2\xi_4}(-k'), \quad (\text{S11})$$

where  $\Delta$  is the gap function and  $\Gamma^a$  is obtained by

$$\Gamma_{\xi_1\xi_2\xi_3\xi_4}^a(k-k') = U_{\xi_1\xi_2\xi_3\xi_4}/2 + U_{\xi_1\xi_2\xi_5\xi_6}\chi_{\xi_5\xi_6\xi_7\xi_8}(k-k')U_{\xi_7\xi_8\xi_3\xi_4}. \quad (\text{S12})$$

Here we adopted abbreviated notation  $k = (\mathbf{k}, i\omega_n)$ . Evaluating  $\lambda$ , eigenvalues of the linearized Éliashberg equation, we determine the critical temperature  $T_c$  from the criterion  $\lambda = 1$ .

### S3. MULTIPOLE SUSCEPTIBILITY

In Fig. S1, we show the magnetic field dependence of the maximum of multipole susceptibility for  $\alpha/t_\perp = 0, 1, 2, 3$ . Figure S1(c) is the same as Fig. 2(a) in the main text. In the left panels, transverse and longitudinal magnetic susceptibilities are shown. In the right panels, the other multipole susceptibilities are shown. Regardless of the value of  $\alpha/t_\perp$ , the transverse (longitudinal) magnetic susceptibility is enhanced (reduced) by the magnetic field, and the susceptibilities for other multipole operators are negligibly small.

### S4. EIGENVALUES OF ÉLIASHBERG EQUATION

In Fig. S2, we show the magnetic field dependence of the eigenvalues of Éliashberg equation for  $\alpha/t_\perp = 0, 1, 2, 3$ . Figure S2(c) is equivalent to Fig. 3(a) in the main text.

### S5. ÉLIASHBERG EQUATION WITHOUT FIELD-ENHANCED MAGNETIC ANISOTROPY

In Fig. S3, we show the magnetic field dependence of the eigenvalues of Éliashberg equation with and without field-enhanced magnetic anisotropy for  $\alpha/t_\perp = 0, 1, 2, 3$ . Figure S3(c) is shown as Fig. 6 in the main text. As shown by the gray dashed lines, the parity transition points are not affected by the field-enhanced magnetic anisotropy. We see that the effect of the field-enhanced magnetic anisotropy becomes remarkable with increasing the spin-orbit coupling  $\alpha$ . Thus, the field dependence of the pairing interaction is closely related to the spin-orbit coupling.

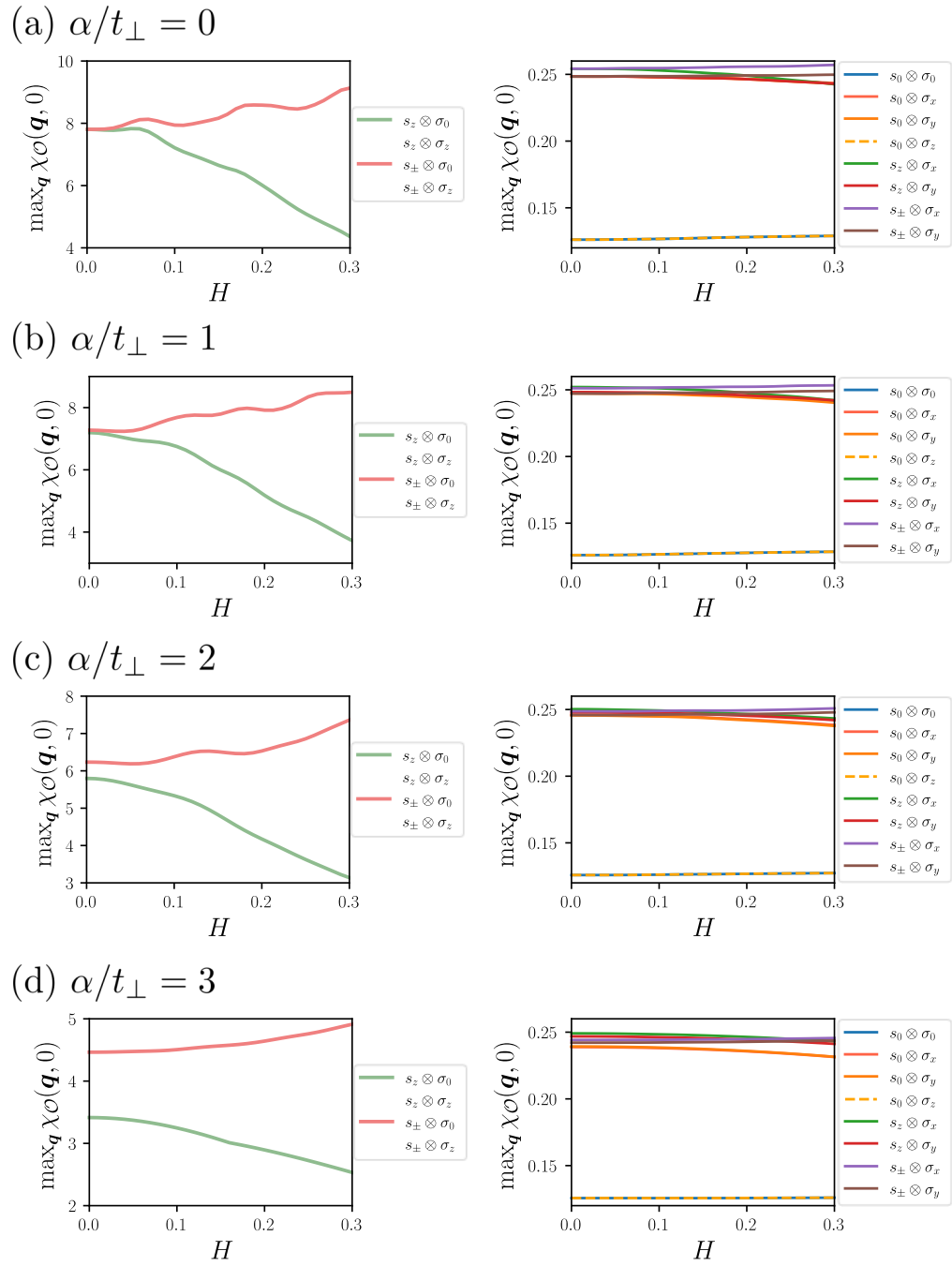


FIG. S1. (a-d) The magnetic field dependence of static multipole fluctuations for  $\alpha/t_{\perp} = 0, 1, 2, 3$ . We set  $T = 0.01$ .

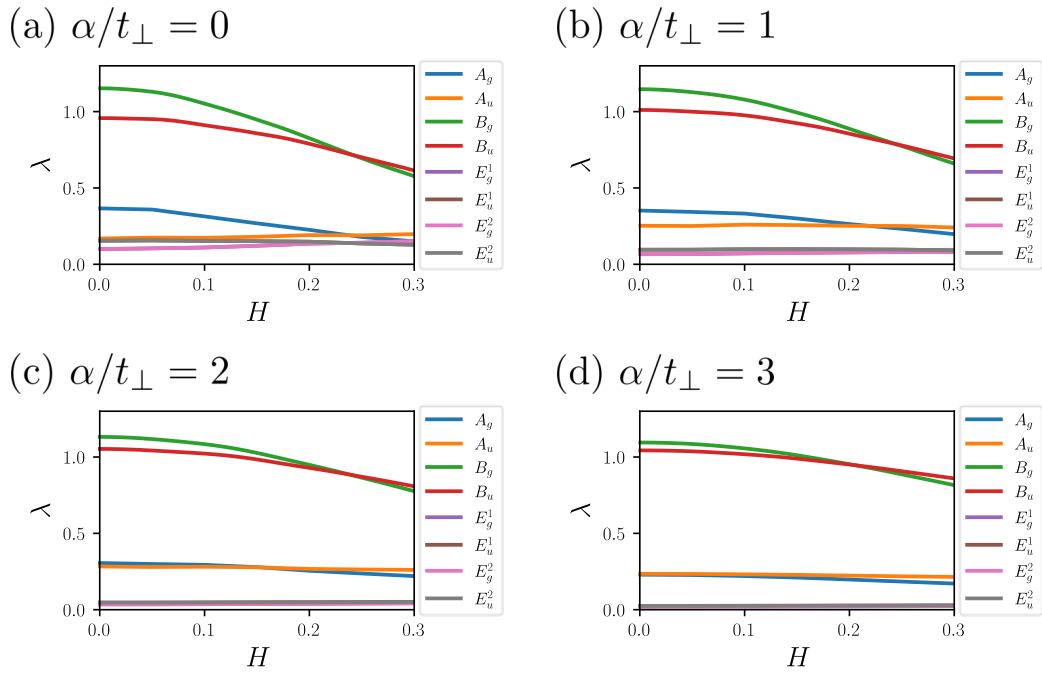


FIG. S2. (a-d) The magnetic field dependence of the eigenvalues of Éliashberg equation for each irreducible representation. We adopt  $\alpha/t_{\perp} = 0, 1, 2, 3$  and fix the temperature  $T = 0.01$ .

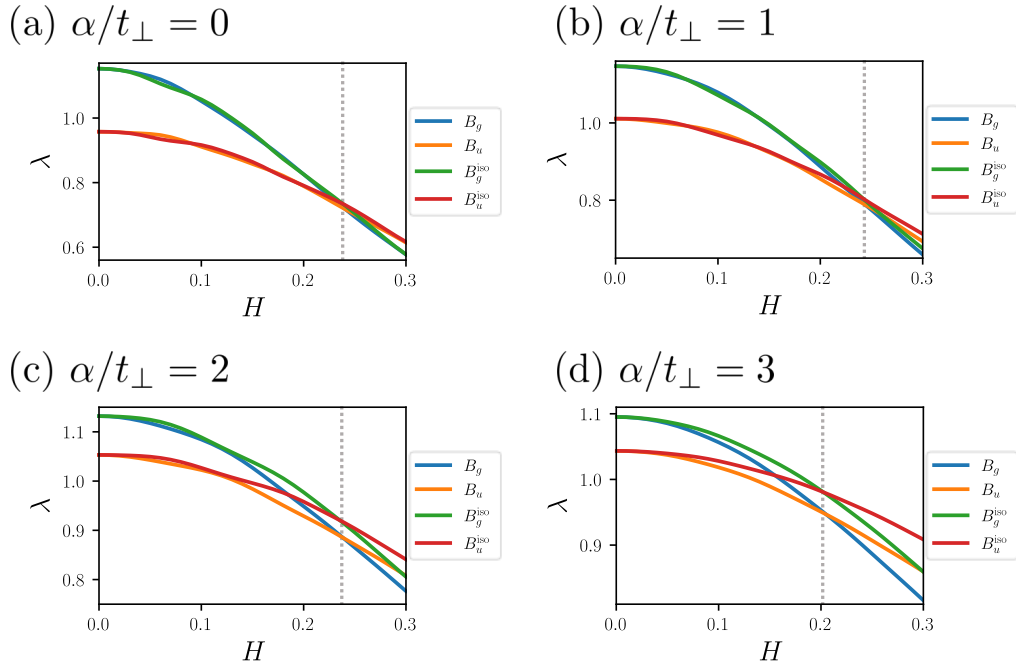


FIG. S3. (a)-(d) The magnetic field dependence of the eigenvalues of Éliashberg equation for the  $B_g$  and  $B_u$  representations. We fix the temperature  $T = 0.01$  and show the results for  $\alpha/t_{\perp} = 0, 1, 2, 3$ .  $B_g^{\text{iso}}$  and  $B_u^{\text{iso}}$  represent the eigenvalues obtained by neglecting the field-enhanced magnetic anisotropy. Details of the calculations are described in the main text. The parity transition points are indicated by the gray dashed lines.